International Journal of Nanomedicine

Dovepress
open access to scientific and medical research

Open Access Full Text Article

ORIGINAL RESEARCH

Incorporation of ROS-Responsive Substance P-Loaded Zeolite Imidazolate Framework-8 Nanoparticles into a Ca^{2+}-Cross-Linked Alginate/Pectin Hydrogel for Wound Dressing Applications

This article was published in the following Dove Press journal:
International Journal of Nanomedicine

Yiming Zhu[1]
Zuochao Yao[2]
Yushu Liu[3]
Wen Zhang[2]
Lele Geng[2]
Tao Ni[2]

[1]Department of General Surgery, Shanghai Ninth People's Hospital, School of Medicine, Shanghai Jiao Tong University, Huangpu, Shanghai, China; [2]Department of Plastic and Reconstructive Surgery, Shanghai Ninth People's Hospital, School of Medicine, Shanghai Jiao Tong University, Huangpu, Shanghai, China; [3]Department of Burns and Plastic Surgery, Binzhou Medical University Hospital, Binzhou City, Shandong Province, China

Purpose: Wound healing, especially of extensive full-thickness wounds, is one of the most difficult problems in clinical studies. In this study, we prepared a novel substance P (SP)-delivery system using zeolite imidazolate framework-8 (ZIF-8) nanoparticles.

Methods: We synthesized ZIF-8 nanoparticles using a modified biomimetic mineralization method. We then coated SP-loaded ZIF-8 nanoparticles (SP@ZIF-8) with polyethylene glycol-thioketal (PEG-TK) to fabricate SP@ZIF-8-PEG-TK nanoparticles, and encapsulated them in injectable hydrogel composed of sodium alginate and pectin and cross-linked using calcium chloride. The final hydrogel wound dressing containing SP@ZIF-8-PEG-TK nanoparticles was called SP@ZIF-8-PEG-TK@CA.

Results: The fabricated ZIF-8 nanoparticles had high SP-loading efficiency. SP-release assay showed that the SP@ZIF-8-PEG-TK nanoparticles maintained drug activity and showed responsive release under stimulation by reactive oxygen species. The SP@ZIF-8-PEG-TK nanoparticles promoted proliferation of human dermal fibroblasts, up-regulated expression levels of inflammation-related genes in macrophages, and exhibited favorable cytocompatibility in vitro. Full-thickness excision wound models in vivo confirmed that SP@ZIF-8-PEG-TK@CA dressings had excellent wound-healing efficacy by promoting an early inflammatory response and subsequent M2 macrophage polarization in the wound-healing process.

Conclusion: In conclusion, these findings indicated that SP@ZIF-8-PEG-TK@CA dressings might be useful for wound dressing applications in the clinic.

Keywords: substance P, metal-organic framework, nanoparticles, hydrogel, wound healing

Introduction

The skin is the body's largest organ and encloses all the other organs in the human body. It functions as a barrier between the outside and internal environments to protect the body from external injury and invasion, and to prevent the loss of nutrients, electrolytes, and body fluids.[1–3] Breaking the barrier may, thus, have serious implication for human health and life.[3]

Numerous strategies have been developed and applied for wound-healing repair, including electrospun nanofibers of cellulose acetate,[4] self-assembled tripeptide glycyl-L-lysine nanoparticles,[5] curcumin loaded sodium hyaluronate immobilized vesicles,[6] allantoin-incorporated organ oil enriched liposomes[7] and tocopherol-loaded vesicle

Correspondence: Tao Ni
Department of Plastic and Reconstructive Surgery, Shanghai Ninth People's Hospital, School of Medicine, Shanghai Jiao Tong University, No. 639 Zhizaoju Road, Huangpu District, Shanghai 200011, People's Republic of China
Email prsnt123456@126.com

submit your manuscript | www.dovepress.com
DovePress
http://doi.org/10.2147/IJN.S225197

transfersomes.[8] Notably, wound healing, especially of extensive full-thickness wounds usually takes a long time.[3] There is, thus, an urgent need for an efficient wound dressing that can promote wound closure, accelerate wound healing, and reduce scar formation.[9,10] In addition, wound dehydration can destroy the conditions needed for injury repair, and the ideal wound dressing should thus also maintain a moist environment to promote wound healing. To date, researchers have developed various wound dressings, such as hydrogels,[11,12] glass microfibers,[10] polycaprolactone,[13] nanofibers[14] and silk fibroin.[15] Hydrogel dressings are widely applied because of their advantages of maintaining oxygen permeation, absorbing tissue exudates, cooling the injury surface to relieve patient discomforts, and thus maintaining a favorable environment for wound-healing progression.[16–19] Injectable hydrogel dressings in particular have unique properties, including in situ drug encapsulation, and attachment and padding to the shape of the wound, thus protecting the injured skin from the outside environment.[20] In addition, stimuli-responsive bio-based polymeric systems have attracted significant attention for diverse biomedical applications.[21,22] However, reactive oxygen species (ROS)-responsive wound dressings have not yet been developed.

Sodium alginate is a natural linear polysaccharide mainly extracted from brown algae,[23] while pectin is also a linear polysaccharide polymer, which can be extracted from diverse plant materials.[24,25] Their characteristics of biocompatibility, biodegradability, and film-forming ability mean that the combination of sodium alginate and pectin (SA/PC hydrogel) has been widely used for wound dressings.[26] However, sodium alginate and pectin lose their shape and integrity when exposed to the physiologic environment due to their hydrophilic nature.[27] Fortunately, ionic crosslinking, especially by Ca^{2+}, can improve the polymers' properties by enhancing their stability, tensile strength, and light transmission and decreasing water-vapor permeation.[26,28] SA/PC hydrogels were therefore selected and subjected to cross-linking by Ca^{2+} for the fabrication of wound dressings.

Substance P (SP) is a 10-amino acid neuropeptide generated by both immune and neuronal cells. It is mainly found in the junction between the adventitia and media in the muscle layer, in connective tissues around blood vessels and in the epidermis and dermis. SP has been shown to regulate wound healing and inflammation.[29,30] It is also an endogenous damage-induced factor that mobilizes CD29 (+) stromal-like cells into the circulation and accelerates wound healing.[31–33]

Metal-organic frameworks (MOFs) are highly crystalline materials combining metal ions or clusters with rigid organic ligands and represent promising materials for biomedical applications.[34] Due to their excellent characteristics of high surface area and porosity, tunable pore shape and size, adjustable structure, biodegradability, and variable internal traits depending on the guest molecules, MOFs have been selected for various applications, including catalysis, gas storage and delivery, selective gas absorption and separation, and drug delivery.[34,35] Notably, the emerging MOF zeolite imidazolate framework-8 (ZIF-8) has attracted wide attention. ZIF-8 has a high loading efficiency and is thus widely used for drug delivery,[36–40] and has also been used as an enhanced delivery system for nucleic acids,[41] oligodeoxynucleotides[42] and proteins.[43,44] However, to the best of our knowledge, ZIF-8 has not yet been developed as a carrier for the delivery of SP for wound healing. We, therefore, loaded ZIF-8 with SP to enhance its delivery to wound sites.

In this study, SP-loaded ZIF-8 (SP@ZIF-8) nanoparticles were fabricated and coated with polyethylene glycol-thioketal (PEG-TK) to obtain a ROS-responsive trait. The obtained SP@ZIF-8-PEG-TK nanoparticles were loaded into a hydrogel consisting of sodium alginate and pectin, and then cross-linked using calcium chloride. ZIF-8 and SP@ZIF-8-PEG-TK nanoparticles were characterized by scanning and transmission electron microscopy, and by Brunauer-Emmett-Teller (BET) and thermogravimetric (TGA) analyses. The ROS-responsiveness of SP@ZIF-8-PEG-TK nanoparticles was assessed by drug-release assay. The effects of the SP@ZIF-8-PEG-TK nanoparticles on human dermal fibroblasts (HDFs) and macrophages were evaluated in vitro. The above resulting SP@ZIF-8-PEG-TK@CA dressing was characterized by scanning and transmission electron microscopy. The dressing with improved properties was used as wound dressing and its function was confirmed in vivo using a full-thickness excision wound model.

Materials and Methods

Fabrication of SP@ZIF-8 Nanoparticles and Dressings

SP@ZIF-8 nanoparticles were synthesized as described previously.[45] Firstly, 0.75 mg SP was added into 0.9 mL aqueous solution of 2-methylimidazolate (MeIM, 3.15 mmol) with vigorous stirring, and the mixture was stirred constantly for 10 min at 30°C, followed by the addition of 0.1 mL aqueous solution of $Zn(NO_3)_2$▪$6H_2O$ (0.045 mmol) and agitation for

10 min at 30°C. SP@ZIF-8 nanoparticles were finally obtained after centrifugation at 3500 rpm for 20 min. Free SP on the surface of the SP@ZIF-8 nanoparticles was removed by rinsing several times with ethanol followed by 5% sodium dodecyl sulfate (w/w) at 50°C. The pure SP@ZIF-8 nanoparticles were lyophilized, weighed, and stored at 4°C.

PEG-TK-coated SP@ZIF-8 (SP@ZIF-8-PEG-TK) nanoparticles were prepared by mixing 50 mg SP@ZIF-8 nanoparticles with 2 mL PEG-TK (25 mg/mL) and then stirring in an ice bath for 10 min. The SP@ZIF-8-PEG-TK nanoparticles were separated from the solution by centrifugation at 12,000 rpm for 5 min. The SP@ZIF-8 -PEG-TK nanoparticles were lyophilized, weighed and stored at 4°C.

SP@ZIF-8-PEG-TK-loaded alginate/pectin-based (SP @ZIF-8-PEG-TK@CA) dressings were fabricated as described previously.[26] Briefly, 1.5 g sodium alginate and 1.5 g pectin were dissolved separately in water, and 0.5 g SP@ZIF-8-PEG-TK was added to each obtained solution and stirred rapidly for 3 h. The above alginate/SP@ZIF-8-PEG-TK and pectin/SP@ZIF-8-PEG-TK solutions were then mixed and 1.5 mL glycerol was added, followed by rapid stirring. SP@ZIF-8-PEG-TK-loaded alginate/pectin gels were poured into petri plates and dried at 45°C for 48 h in an oven. SP@ZIF-8-loaded alginate/pectin dressings were then obtained. SP-loaded alginate/pectin (SP@CA) dressings were prepared using a similar method.

For cross-linking, the above SP@ZIF-8-PEG-TK@CA dressings were dipped in 0.5% w/v calcium chloride solution containing 7% v/v glycerol to fabricate ionic cross-linked SP@ZIF-8-PEG-TK@CA dressings.

Characterization

ZIF-8 nanoparticle (100 μg/mL) and SP@ZIF-8-PEG-TK nanoparticle solutions (100 μg/mL) were prepared separately by diluting in double distilled water and characterized. The ultrastructures of the ZIF-8 and SP@ZIF-8-PEG-TK nanoparticles were examined by scanning electron microscopy (SEM, Hitachi FE-SEM S-4800) and transmission electron microscopy (TEM, JEM-2100F). The particle sizes of the ZIF-8 and SP@ ZIF-8 nanoparticles were measured by dynamic light scattering (DLS) at 25°C using a Malvern Zetasizer NanoZS instrument. The BET surface areas of the ZIF-8 and SP@ ZIF-8 nanoparticles were examined by N_2 adsorption-desorption. TGA of the ZIF-8 and SP@ZIF-8-PEG-TK nanoparticles was performed using a TAQ500 thermogravimetric analyzer, and the data were obtained from 25~800°C increasing at 10°C/min of scan rate.

SP-Release Assay

We explored the effects of ROS on SP release from SP@ZIF-8-PEG-TK nanoparticles by drug-release assays in phosphate buffer (PBS, pH 7.4) containing different concentrations of H_2O_2 (0, 5, and 20 mM) at 37°C. SP@ZIF-8-PEG-TK nanoparticles (50 mg) were added into the buffer (10 mL) and the mixture was shaken mildly (50 rpm/min) for 48 h. The fluorescence intensity of the solution was then read at intervals with a Lambda Bio40 UV/visspectrometer (Perkin-Elmer).

Cell Culture

HDFs and RAW264.7 macrophages were purchased from Kunming Animal Institute. HDFs were maintained in Dulbecco's Modified Eagle Medium containing 100 μg/mL streptomycin, 100 U/mL penicillin, and 10% fetal bovine serum (FBS). RAW264.7 macrophages were maintained in α-Minimal Essential Medium supplemented with 100 U/mL penicillin and 10% FBS. All cells were cultured in an atmosphere of 37°C and 5% CO_2. Raw264.7 macrophages were stimulated with lipopolysaccharide (LPS) to induce M1 phenotype macrophages.

Cell Proliferation

The viability of HDFs treated with SP alone or SP@ZIF-8-PEG-TK nanoparticles was determined by the cell counting kit-8 (CCK-8) assay. HDFs (2.0×10^4 cells/cm^2) were plated on a cell culture dish and the absorbance was detected by spectrophotometry after 1, 4 and 7 days of incubation, using a microplate reader at a wavelength of 450 nm.

Cell Spreading

HDFs were incubated with SP, ZIF-8 and SP@ZIF-8-PEG-TK nanoparticles and their morphologies were observed by confocal laser scanning microscopy (CLSM). HDFs were collected after 24 h of incubation, fixed for 30 min with 4% paraformaldehyde, and then stained with rhodamine-labelled phalloidin (Abcam) for 45 min, followed by DAPI (Sigma) for 10 min. Finally, the cells were rinsed with PBS and observed by CLSM to visualize the nuclei and cytoskeleton.

Real-Time Quantitative Polymerase Chain Reaction (RT-qPCR)

The expression levels of inflammation-related genes in LPS-induced macrophages with or without SP@ZIF-8-PEG-TK

treatment were determined by RT-qPCR. The primer sequences are shown in Table 1.

In vivo Full-Thickness Excision Wound Healing Mouse Model

BALB/c mice (4 weeks old) were used in the animal study. All animal experiments were approved by the Animal Ethics Committee of Shanghai Ninth People's Hospital, School of Medicine, Shanghai Jiao Tong University and carried out in accordance with its guidelines. The mice were anesthetized by intraperitoneal injection of pentobarbitone sodium (50 mg/kg). Their backs were then shaved, the exposed skin was sterilized with 75% ethanol, and a full-thickness wound (diameter 1 cm) was incised on the exposed dorsum. The wound was then treated with 100 μL of SP@CA or SP@ZIF-8-PEG-TK@CA dressings and covered with a bandage. Wound healing was observed 3, 7 and 15 days post-wounding. The reduction wound area was calculated according to the following equation:

$$\text{Wound area reduction}(\%) = (\text{Ai} - \text{At})/\text{Ai} \times 100\%$$

Where Ai is the initial wound area and At is the area of the wound at a specific time point.

Table 1 Primer Sequences Used in RT-qPCR

Gene	Primer Sequences (5′–3′)	Product Size (bp)
IL-6	Forward: AGGCACTCCCCCAAAAGATG	250
	Reverse: TTTGCTACGACGTGGGCTAC	
IL-1β	Forward: GTCCTTCCTACCCCAATTTCCA	151
	Reverse: CGCACTAGGTTTGCCGAGTA	
iNOS	Forward: GGAAGCCTGGATCGTACCTG	289
	Reverse: TCACCCTCTCCCCAGAAACT	
GAPDH	Forward: CCCTTAAGAGGGATGCTGCC	263
	Reverse: ACTGTGCCGTTGAATTTGCC	

Immunofluorescence Analysis

After different treatments, HDFs or wound tissues were collected and fixed with 4% paraformaldehyde. M1 and M2 phenotype macrophages were detected in HDFs or wound tissues sections after staining with CD32 and CD206 (Santa Cruz Biotecknology), respectively. DAPI (Sigma) was used to stain the nuclei.

Statistical Analysis

The data were recorded as mean ± standard deviation. Statistical analysis was carried out using IBM SPSS Statistics (version 20.0). Comparisons between two groups were made using Student's *t*-test and comparisons among multiple groups by one-way analysis of variance followed by Turkey's test. $P<0.05$ indicated a significant difference.

Results and Discussion

Fabrication and Characterization of SP@ZIF-8-PEG-TK Nanoparticles

Using a biomimetic mineralization approach, SP was embedded in porous ZIF-8 nanoparticles by incubation with MeIM and $Zn(NO_3)_2$▪$6H_2O$. The SP@ZIF-8 was then coated with PEG-TK to prepare SP@ZIF-8-PEG-TK nanoparticles. The morphological characteristics of the ZIF-8 nanoparticles and SP@ZIF-8-PEG-TK composite nanoparticles were determined by TEM and SEM, respectively (Figure 1A–D). Representative SEM images demonstrated that SP@ZIF-8-PEG-TK nanoparticles were rhombic and uniformly dodecahedral, similar to blank ZIF-8. Representative TEM images of ZIF-8 and SP@ZIF-8-PEG-TK also showed similarly morphological characteristics, suggesting that the encapsulation of SP into ZIF-8 nanoparticles did not affect the nanoparticles' morphology.

The diameters of the ZIF-8 and SP@ZIF-8-PEG-TK nanoparticles were 101.1 ± 8.5 and 165.3 ± 24 nm, respectively, as measured by DLS (Figure 1E). BET analysis of ZIF-8 and SP@ZIF-8-PEG-TK nanoparticles by N_2 adsorption-desorption showed that the surface area of ZIF-8 was 1332 m^2/g, while the surface area of SP@ZIF-8-PEG-TK decreased to 731 m^2/g (Figure 1F), indicating that SP was successfully loaded into the SP@ZIF-8-PEG-TK nanoparticles. TGA estimated that the loading capacity of SP@ZIF-8-PEG-TK for SP was about 49.3 μg/mg (i.e., 1 mg SP@ZIF-8 nanoparticles loaded about 49.3 μg SP) (Figure 1G).

In this study, SP@ZIF-8 was coated by PEG-TK through ROS-responsive TK linkers. Stimulation with ROS would

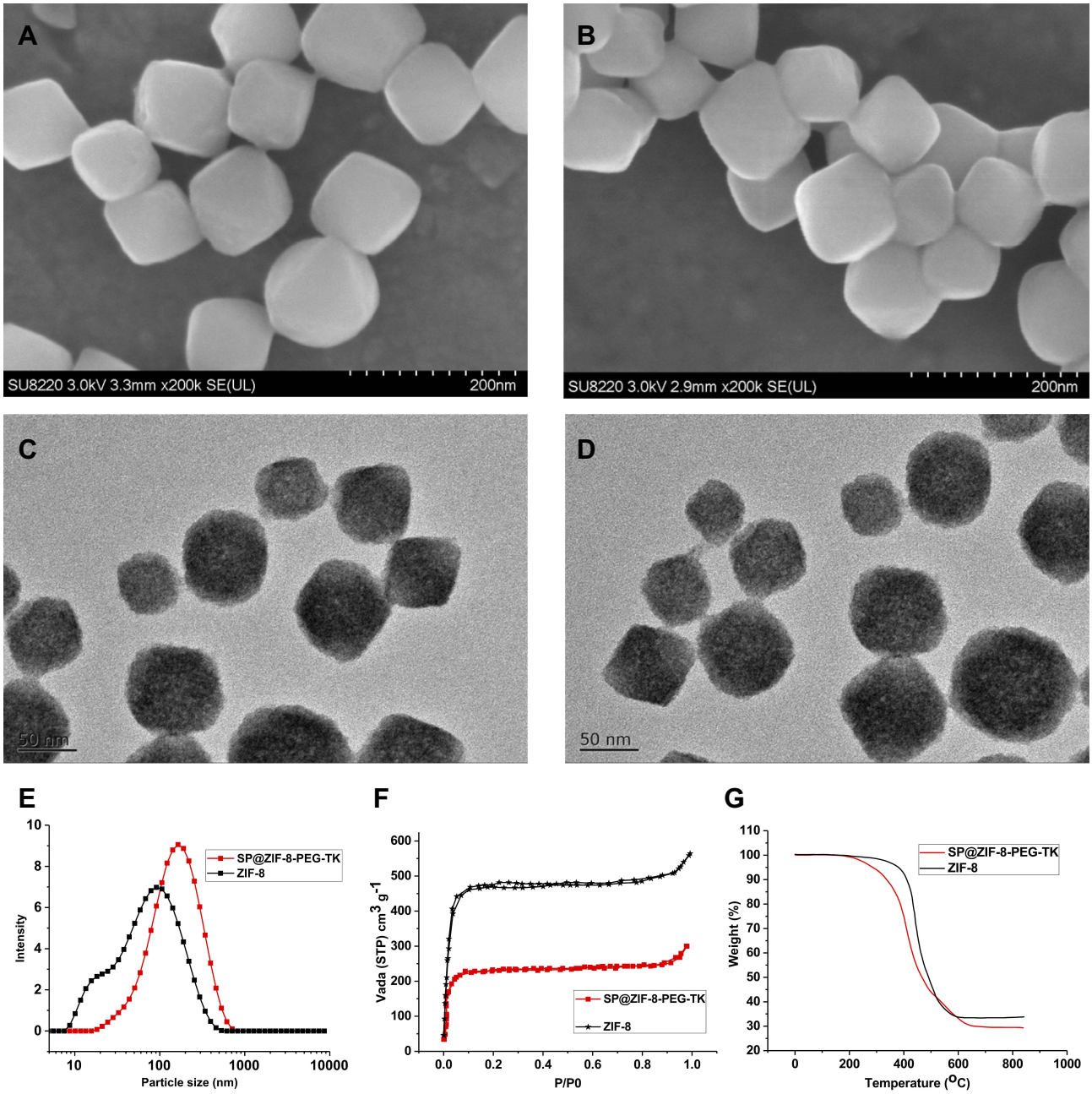

Figure 1 Characterization of ZIF-8 and SP@ZIF-PEG-TK nanoparticles. Typical SEM images of ZIF-8 (**A**) and SP@ZIF-8-PEG-TK (**B**). Typical TEM images of ZIF-8 (**C**) and SP@ZIF-8-PEG-TK (**D**). (**E**). Particle sizes of ZIF-8 and SP@ZIF-8-PEG-TK. (**F**). N_2 adsorption-desorption isotherm for ZIF-8 and SP@ZIF-8-PEG-TK. (**G**). TGA curves recorded for ZIF-8 and SP@ZIF-8-PEG-TK.

break the TK linkers, leading to the release of the loaded drug from the pores of the nanoparticles. We explored the ROS-responsiveness of the SP@ZIF-8-PEG-TK nanoparticles using the typical ROS stimulus H_2O_2, and detected the SP-release curves from the SP@ZIF-8-PEG-TK nanoparticles in PBS containing different concentrations of H_2O_2 by spectro fluorophotometry. SP@ZIF-8 was effectively gated by PEG-TK in the absence of H_2O_2, and < 20% of SP was released even after 48 h of incubation, indicating a high efficiency of anchoring of nanovalves through the TK linkers. In contrast, 45% of the SP was released after incubation with 5 mM H_2O_2 for 48 h, and >90% of SP was released after incubation with 10 mM H_2O_2 for 48 h. The H_2O_2 concentration, thus, had a positive and significant impact on the release rate of SP from SP@ZIF-8-PEG-TK nanoparticles. These findings revealed that the TK linkers acted as a nanovalve and opened the pores following ROS stimulation (Figure 2). ROS are known to be generated at wound sites.[46,47] These nanoparticles could thus sustainably

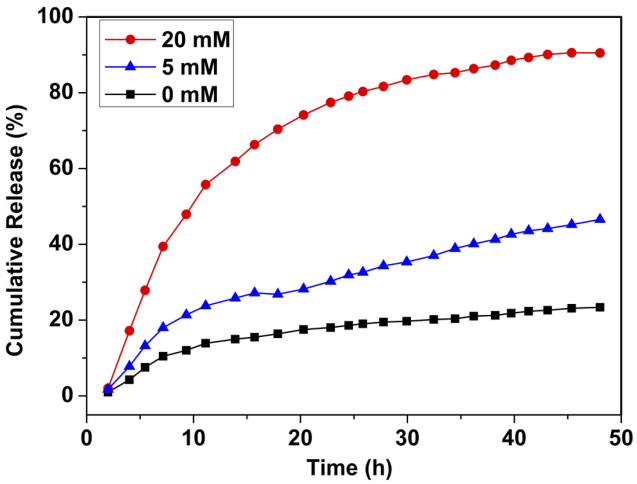

Figure 2 The SP release profiles of SP@ZIF-8-PEG-TK nanoparticles incubated with different concentrations of H_2O_2.

release SP in an incisional wound microenvironment containing high levels of ROS.

SP@ZIF-8-PEG-TK Nanoparticles Promoted HDFs Proliferation

To investigate the effects of SP@ZIF-8-PEG-TK nanoparticles on the proliferation of HDFs, we incubated HDFs with SP alone or SP@ZIF-8-PEG-TK nanoparticles and determined their viability by CCK-8 assay. There was no significant difference among the three groups after 1 and 4 days of culture (Figure 3). However, the SP and SP@ZIF-8-PEG-TK groups showed significantly higher cell viabilities than the control group by 7 days, and the viability of the SP@ZIF-8-PEG-TK group was higher than that of the SP group. These finding indicated that SP@ZIF-8-PEG-TK nanoparticles promoted the proliferation of HDFs.

We observed the spreading of HDFs cultured with SP, ZIF-8 and SP@ZIF-8-PEG-TK nanoparticles by CLSM (Figure 4). All the HDFs possessed a typical shape and had abundant actin filaments linking them to the surrounding cells after 24 and 72 h of incubation. However, the density and morphological characteristic of the HDFs treated with SP and SP@ZIF-8-PEG-TK were superior to those without treatment or treated with pure ZIF-8 nanoparticles after 72h of incubation.

Inflammation-Related Gene Expression

LPS activates macrophages and induces inflammation-related genes, including inducible nitric oxide synthase (iNOS), interleukin-6 (IL-6), and interleukin-1β (IL-1β).[48,49] These activated macrophages are called M1 phenotype macrophages. We determined the expression levels of these inflammation-

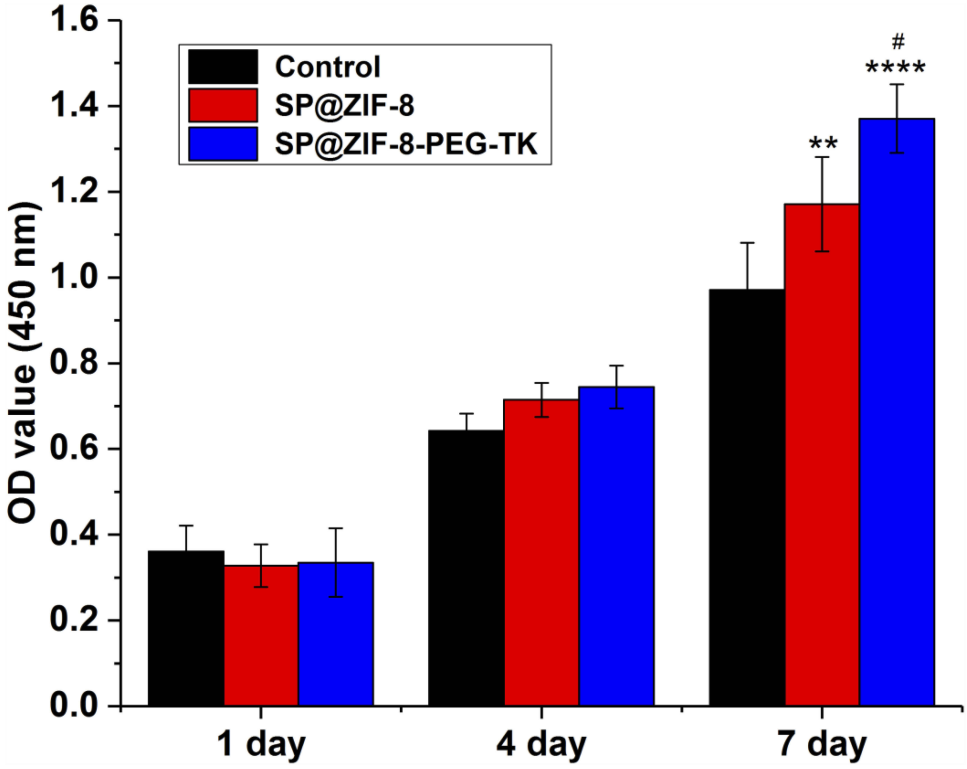

Figure 3 Cell viability of human dermal fibroblasts (HDFs) incubated with SP or SP@ZIF-8-PEG-TK nanoparticles. **P<0.01, ****P<0.0001 vs Control group; #P<0.05 vs SP group.

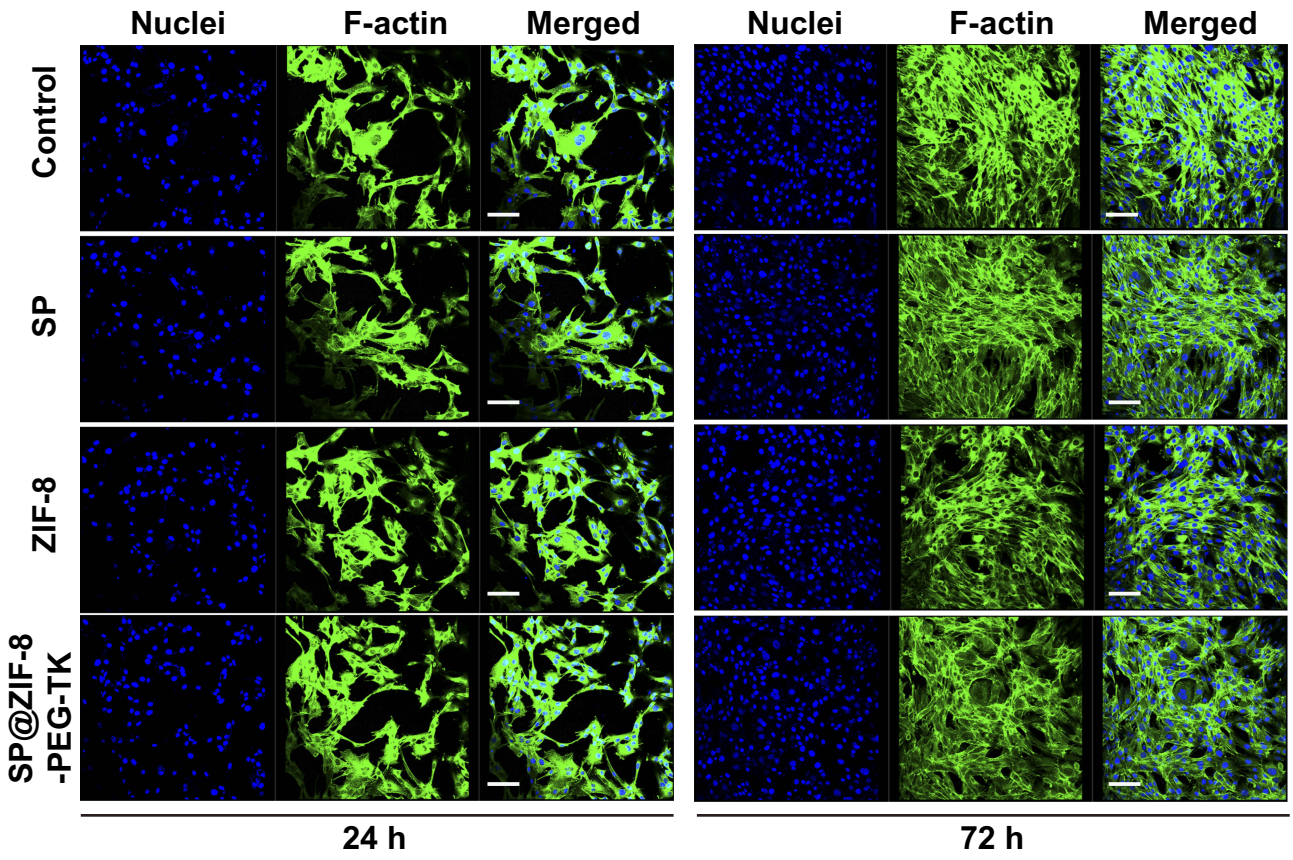

Figure 4 Confocal laser scanning microscopy (CLSM) observations of HDFs cells incubated with SP, ZIF-8 and SP@ZIF-8-PEG-TK for 24 h and 72 h. For each panel, the images from left to right showed cell nuclei stained by DAPI (blue), FITC fluorescence in cells (green) and the merged one of the left two images. Scale bar, 100 μm.

related genes in macrophages after 24 h of treatment with SP or SP@ZIF-8-PEG-TK nanoparticles, using RT-qPCR. The levels of IL-6, IL-1β, and iNOS mRNA were significantly elevated after treatment with SP@ZIF-8-PEG-TK nanoparticles, suggesting that the nanoparticles had pro-inflammatory effects (Figure 5).

SP@ZIF-8-PEG-TK Nanoparticles Promoted the Transfer to M2 Macrophages

CD32 is a marker of M1 phenotype macrophages.[50] In the current study, the immunofluorescence intensity of CD32 was increased in cells treated with SP@ZIF-8-PEG-TK nanoparticle compared with the control and SP treatments, suggesting

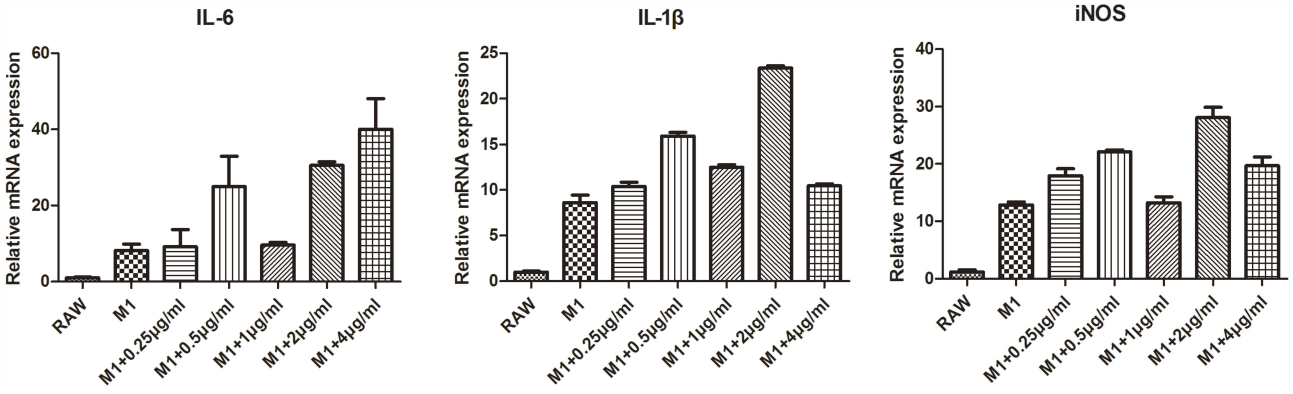

Figure 5 The expression of inflammation-related genes in LPS-induced macrophages (M1) after 24 h of treatment by different concentration of SP@ZIF-8-PEG-TK nanoparticles.
Abbreviations: RAW, Raw264.7 macrophages; M1, Raw264.7 macrophages induced by lipopolysaccharide; IL-6, interleukin-6; IL-1β, interleukin-1β; iNOS, inducible nitric oxide synthase.

the generation of M1 phenotype macrophages (Figure 6). An increase in M1 phenotype macrophages indicated the pro-inflammatory effect of SP@ZIF-8-PEG-TK nanoparticles and their consequent potential for wound healing.

Characterization of SP@ZIF-8-PEG-TK @CA Dressings

SEM images of cross-sections of SP@CA and SP@ZIF-8-PEG-TK@CA dressings are shown in Figure 7. Both dressings had an interconnected porous architecture. The addition of SP@ZIF-8-PEG-TK had no significant effect on the pore size or interconnection between the pores of the hydrogel dressings. The SP@ZIF-8-PEG-TK nanoparticles were dispersed homogeneously as primary particles in the polymer matrix of the hydrogel films.

In vivo Wound Healing

We investigated the healing functions of SP@CA and SP @ZIF-8-PEG-TK@CA in an infected cutaneous wound mouse model in vivo. Photographs of wound treated with SP@CA and SP@ZIF-8-PEG-TK@CA for 3, 7 and 15 days are shown in Figure 8. SP@ZIF-8-PEG-TK@CA

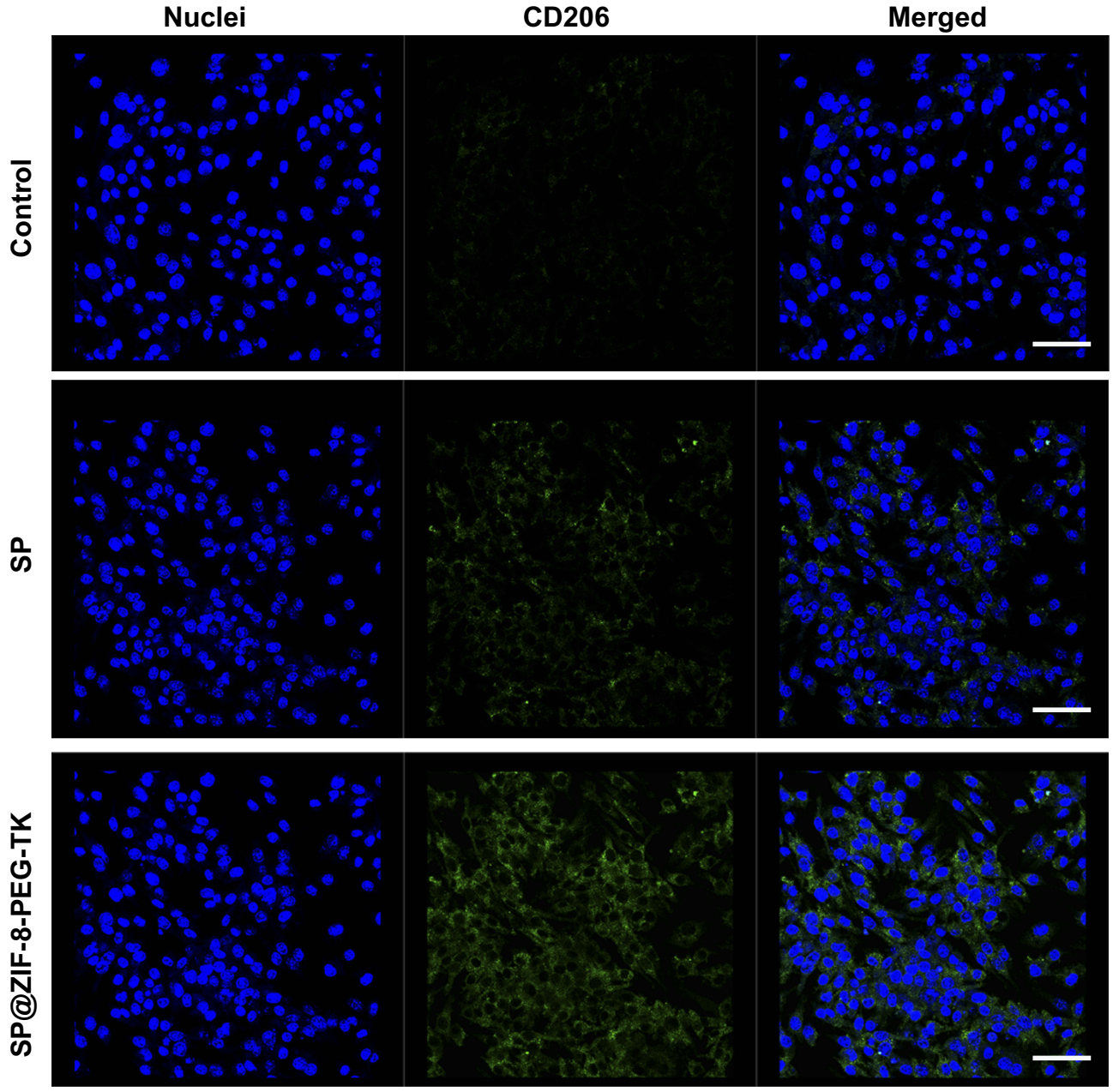

Figure 6 The expression of CD32 in macrophages treated by SP or SP@ZIF-8-PEG-TK nanoparticles. Scale bar, 100 μm.

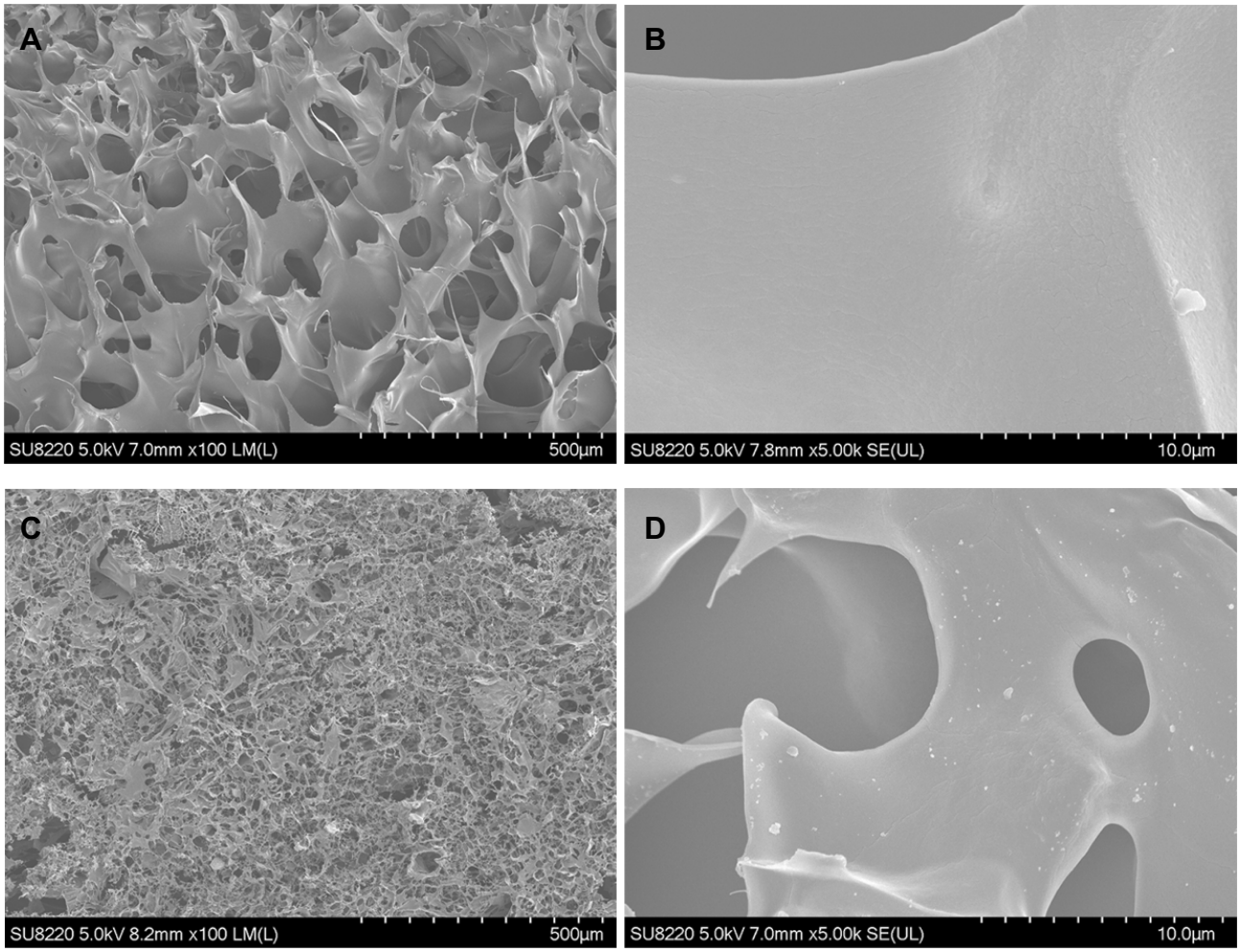

Figure 7 Morphologies of SP-loaded ionic cross-linked alginate/pectin-based (SP@CA) and SP@ZIF-8-PEG-TK-loaded ionic cross-linked alginate/pectin-based (SP@ZIF-8-PEG-TK@CA) dressings. SEM images of SP@CA (**A** and **B**) and SP@ZIF-8-PEG-TK@CA (**C** and **D**) dressings.

reduced the wound area by 12.6% after 3 days, compared with only 5.9% in the SP@CA group (Figure 8). After 7 days of treatment, SP@ZIF-8-PEG-TK@CA had reduced the wound area by 62.5%, which was significantly more than the 42.5% in the SP@CA group. SP@ZIF-8-PEG-TK @CA had almost completely closed the wound (nearly 100%) after 15 days of treatment, which was also significantly higher than in the SP@CA group.

To investigate the mechanism underlying the effects of SP@CA and SP@ZIF-8-PEG-TK@CA dressings at the injured sites, we carried out immunofluorescence staining of CD32 at day 3 and CD206 staining at day 7. There were abundant CD32-positive cells at the injured sites in the SP@ZIF-8-PEG-TK@CA group (Figure 9A). The observed effects of SP@ZIF-8-PEG-TK-CA dressings in vivo were consistent with those of the SP@ZIF-8-PEG-TK nanoparticles in vitro. SP@ZIF-8-PEG-TK@CA dressings promoted an inflammatory response and accelerated wound healing at an early stage of the wound-healing process.

M2 phenotype macrophage, characterized by high expression levels of CD206, are referred to as "wound healing"-macrophages and play an important role in tissue repair.[51–53] In the current study, the numbers of CD206-positive cells at wound sites at the late stage were higher in mice treated with SP@ZIF-8-PEG-TK@CA compared with SP@CA dressings (Figure 9B). All these findings suggested that SP@ZIF-8-PEG-TK@CA stimulated and promoted wound healing by M2 macrophage polarization.[54]

Conclusion

In this study, we developed an injectable hydrogel for wound dressing application and confirmed that this dressing markedly promoted wound healing in a full-thickness excision mouse model. The SP@ZIF-8-PEG-TK@CA hydrogel dressing was

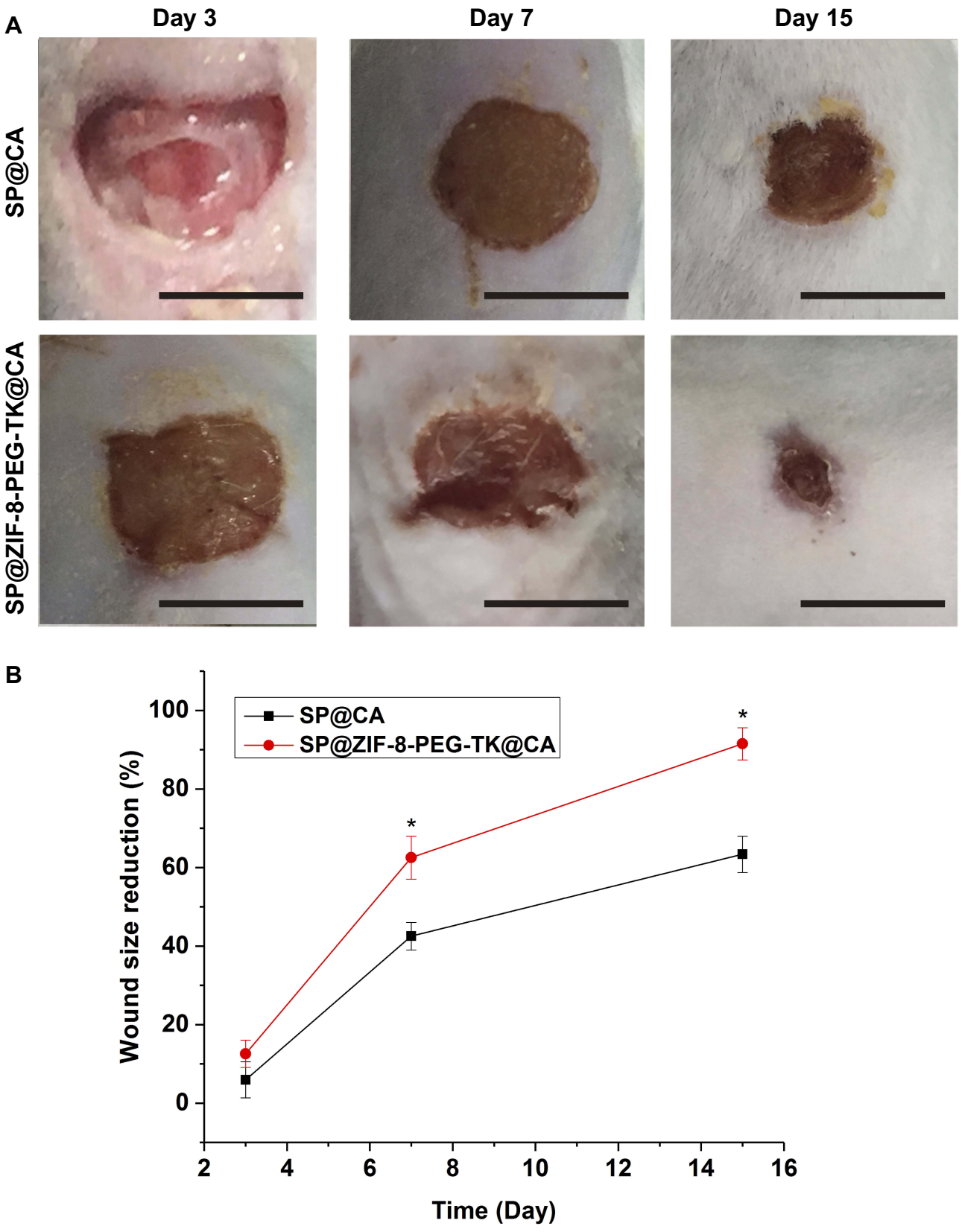

Figure 8 Representative photographs (**A**) of wound treated with SP@CA and SP@ZIF-8-PEG-TK@CA at 3, 7 and 15 days and their corresponding quantitative measurement of wound area reduction (**B**). *P < 0.05; Scale bar, 1 cm.

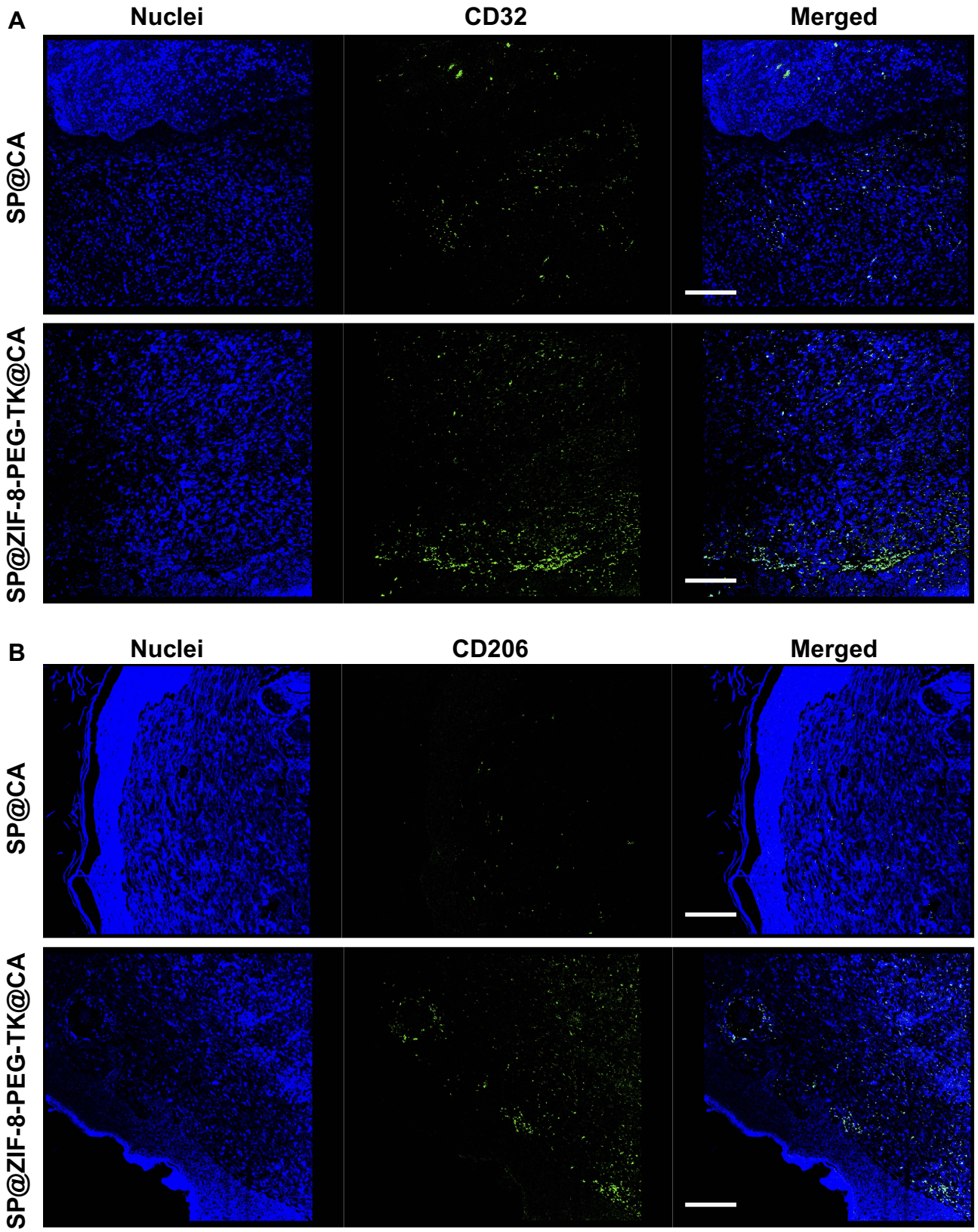

Figure 9 The tissue immunofluorescence staining for the group treated with SP@CA or SP@ZIF-8-PEG-TK@CA. (**A**). CD32 staining for the two groups at day 3. (**B**). CD206 staining for the two groups at day 7. Scale bar, 100 μm.

prepared by incorporating SP-loaded ZIF-8-coated with PEG-TK (SP@ZIF-8-PEG-TK) nanoparticles into a hydrogel consisting of sodium alginate and pectin, and then cross-linked using calcium chloride. The SP@ZIF-8-PEG-TK nanoparticles exhibited high SP-loading efficiency and a novel ROS-stimulus -responsive release. The nanoparticles promoted the proliferation of human dermal fibroblasts, up-regulated the expression of inflammation-related genes in macrophages and exhibited favorable cytocompatibility in vitro. The SP@ZIF-8-PEG-TK @CA dressing also promoted an inflammatory response at the early stage and M2 macrophage polarization at the late stage of the wound-healing process, and thus, exhibited excellent wound-healing efficacy in vivo. Overall, these findings indicate that SP@ZIF-8-PEG-TK@CA dressing might be a promising candidate for clinical wound dressing applications.

Ethics Approval and Consent to Participate

All animal experiments were approved by the Animal Ethics Committee of Shanghai Ninth People's Hospital, School of Medicine, Shanghai Jiao Tong University and carried out in accordance with its guidelines.

Funding

This research was partially supported by National Science Foundation of China for Young Scholars (No. 814011585).

Disclosure

The authors declared that they have no competing interests.

References

1. Biro T, Toth BI, Hasko G, Paus R, Pacher P. The endocannabinoid system of the skin in health and disease: novel perspectives and therapeutic opportunities. *Trends Pharmacol Sci*. 2009;30(8):411–420. doi:10.1016/j.tips.2009.05.004
2. McLafferty E, Hendry C, Alistair F. The integumentary system: anatomy, physiology and function of skin. *Nurs Stand*. 2012;27(3):35–42. doi:10.7748/ns2012.09.27.3.35.c9299
3. Xu R, Luo G, Xia H, et al. Novel bilayer wound dressing composed of silicone rubber with particular micropores enhanced wound re-epithelialization and contraction. *Biomaterials*. 2015;40:1–11. doi:10.1016/j.biomaterials.2014.10.077
4. Liu X, Lin T, Gao Y, et al. Antimicrobial electrospun nanofibers of cellulose acetate and polyester urethane composite for wound dressing. *J Biomed Mater Res B*. 2012;100(6):1556–1565. doi:10.1002/jbm.b.32724
5. Sun L, Li A, Hu Y, Li Y, Shang L, Zhang L. Self-assembled fluorescent and antibacterial GHK-Cu nanoparticles for wound healing applications. *Part Part Syst Char*. 2019;36(4):1800420. doi:10.1002/ppsc.201800420
6. Manca ML, Castangia I, Zaru M, et al. Development of curcumin loaded sodium hyaluronate immobilized vesicles (hyalurosomes) and their potential on skin inflammation and wound restoring. *Biomaterials*. 2015;71:100–109. doi:10.1016/j.biomaterials.2015.08.034
7. Manca ML, Matricardi P, Cencetti C, et al. Combination of argan oil and phospholipids for the development of an effective liposome-like formulation able to improve skin hydration and allantoin dermal delivery. *Int J Pharm*. 2016;505(1–2):204–211. doi:10.1016/j.ijpharm.2016.04.008
8. Caddeo C, Manca ML, Peris JE, et al. Tocopherol-loaded transfersomes: in vitro antioxidant activity and efficacy in skin regeneration. *Int J Pharm*. 2018;551(1–2):34–41. doi:10.1016/j.ijpharm.2018.09.009
9. Agarwal A, Nelson TB, Kierski PR, et al. Polymeric multilayers that localize the release of chlorhexidine from biologic wound dressings. *Biomaterials*. 2012;33(28):6783–6792. doi:10.1016/j.biomaterials.2012.05.068
10. Zhao S, Li L, Wang H, et al. Wound dressings composed of copper-doped borate bioactive glass microfibers stimulate angiogenesis and heal full-thickness skin defects in a rodent model. *Biomaterials*. 2015;53:379–391. doi:10.1016/j.biomaterials.2015.02.112
11. Singh B, Sharma S, Dhiman A. Design of antibiotic containing hydrogel wound dressings: biomedical properties and histological study of wound healing. *Int J Pharm*. 2013;457(1):82–91. doi:10.1016/j.ijpharm.2013.09.028
12. Manconi M, Manca ML, Caddeo C, et al. Preparation of gellan-cholesterol nanohydrogels embedding baicalin and evaluation of their wound healing activity. *Eur j Pharm Biopharm*. 2018;127:244–249. doi:10.1016/j.ejpb.2018.02.015
13. Muwaffak Z, Goyanes A, Clark V, Basit AW, Hilton ST, Gaisford S. Patient-specific 3D scanned and 3D printed antimicrobial polycaprolactone wound dressings. *Int J Pharm*. 2017;527(1–2):161–170. doi:10.1016/j.ijpharm.2017.04.077
14. Sarhan WA, Azzazy HM. Apitherapeutics and phage-loaded nanofibers as wound dressings with enhanced wound healing and antibacterial activity. *Nanomedicine*. 2017;12(17):2055–2067. doi:10.2217/nnm-2017-0151
15. Farokhi M, Mottaghitalab F, Fatahi Y, Khademhosseini A, Kaplan DL. Overview of silk fibroin use in wound dressings. *Trends Biotechnol*. 2018;36(9):907–922. doi:10.1016/j.tibtech.2018.04.004
16. Anumolu SS, Menjoge AR, Deshmukh M, et al. Doxycycline hydrogels with reversible disulfide crosslinks for dermal wound healing of mustard injuries. *Biomaterials*. 2011;32(4):1204–1217. doi:10.1016/j.biomaterials.2010.08.117
17. Gong C, Wu Q, Wang Y, et al. A biodegradable hydrogel system containing curcumin encapsulated in micelles for cutaneous wound healing. *Biomaterials*. 2013;34(27):6377–6387. doi:10.1016/j.biomaterials.2013.05.005
18. Dong Y, Hassan WU, Kennedy R, et al. Performance of an in situ formed bioactive hydrogel dressing from a PEG-based hyperbranched multifunctional copolymer. *Acta Biomater*. 2014;10(5):2076–2085. doi:10.1016/j.actbio.2013.12.045
19. Kamoun EA, Kenawy ES, Chen X. A review on polymeric hydrogel membranes for wound dressing applications: PVA-based hydrogel dressings. *J Adv Res*. 2017;8(3):217–233. doi:10.1016/j.jare.2017.01.005
20. Hamedi H, Moradi S, Hudson SM, Tonelli AE. Chitosan based hydrogels and their applications for drug delivery in wound dressings: a review. *Carbohydr Polym*. 2018;199:445–460. doi:10.1016/j.carbpol.2018.06.114
21. Gao S, Tang G, Hua D, et al. Stimuli-responsive bio-based polymeric systems and their applications. *J Mater Chem B*. 2019;7(5):709–729. doi:10.1039/c8tb02491j
22. Chatterjee S, Chi-Leung Hui P. Review of stimuli-responsive polymers in drug delivery and textile application. *Molecules*. 2019;24(14). doi:10.3390/molecules24142547
23. Wang X, Zhang Y, Liang H, et al. Synthesis and properties of castor oil-based waterborne polyurethane/sodium alginate composites with tunable properties. *Carbohydr Polym*. 2019;208:391–397. doi:10.1016/j.carbpol.2018.12.090

24. Patova OA, Smirnov VV, Golovchenko VV, Vityazev FV, Shashkov AS, Popov SV. Structural, rheological and antioxidant properties of pectins from Equisetum arvense L. and Equisetum sylvaticum L. *Carbohydr Polym*. 2019;209:239–249. doi:10.1016/j.carbpol.2018.12.098
25. Yu N, Wang X, Ning F, et al. Development of antibacterial pectin from Akebia trifoliata var. australis waste for accelerated wound healing. *Carbohydr Polym*. 2019;217:58–68. doi:10.1016/j.carbpol.2019.03.071
26. Shahzad A, Khan A, Afzal Z, Umer MF, Khan J, Khan GM. Formulation development and characterization of cefazolin nanoparticles-loaded cross-linked films of sodium alginate and pectin as wound dressings. *Int J Biol Macromol*. 2019;124:255–269. doi:10.1016/j.ijbiomac.2018.11.090
27. George M, Abraham TE. Polyionic hydrocolloids for the intestinal delivery of protein drugs: alginate and chitosan–a review. *J Controlled Release*. 2006;114(1):1–14. doi:10.1016/j.jconrel.2006.04.017
28. Liling G, Di Z, Jiachao X, Xin G, Xiaoting F, Qing Z. Effects of ionic crosslinking on physical and mechanical properties of alginate mulching films. *Carbohydr Polym*. 2016;136:259–265. doi:10.1016/j.carbpol.2015.09.034
29. Zheng XF, Zhao ED, He JY, Zhang YH, Jiang SD, Jiang LS. Inhibition of substance P signaling aggravates the bone loss in ovariectomy-induced osteoporosis. *Prog Biophys Mol Biol*. 2016;122(2):112–121. doi:10.1016/j.pbiomolbio.2016.05.011
30. Gaddam RR, Chambers S, Murdoch D, Shaw G, Bhatia M. Circulating levels of hydrogen sulfide and substance P in patients with sepsis. *J Infect*. 2017;75(4):293–300. doi:10.1016/j.jinf.2017.07.005
31. Lee JY, Kim WS, Kim W, Kim HK, Bae TH, Park JA. Wound contraction decreases with intravenously injected substance P in rabbits. *Burns*. 2014;40(1):127–134. doi:10.1016/j.burns.2013.06.008
32. Leal EC, Carvalho E, Tellechea A, et al. Substance P promotes wound healing in diabetes by modulating inflammation and macrophage phenotype. *Am J Pathol*. 2015;185(6):1638–1648. doi:10.1016/j.ajpath.2015.02.011
33. Kant V, Kumar D, Prasad R, et al. Combined effect of substance P and curcumin on cutaneous wound healing in diabetic rats. *J Surg Res*. 2017;212:130–145. doi:10.1016/j.jss.2017.01.011
34. Zhao D, Timmons DJ, Yuan D, Zhou HC. Tuning the topology and functionality of metal-organic frameworks by ligand design. *Acc Chem Res*. 2011;44(2):123–133. doi:10.1021/ar100112y
35. Horcajada P, Gref R, Baati T, et al. Metal-organic frameworks in biomedicine. *Chem Rev*. 2012;112(2):1232–1268. doi:10.1021/cr200256v
36. Lai X, Liu H, Zheng Y, Wang Z, Chen Y. Drug loaded nanoparticles of metal-organic frameworks with high colloidal stability for anticancer application. *J Biomed Nanotechnol*. 2019;15(8):1754–1763. doi:10.1166/jbn.2019.2807
37. Ren SZ, Zhu D, Zhu XH, et al. Nanoscale metal-organic-frameworks coated by biodegradable organosilica for pH and redox dual responsive drug release and high-performance anticancer therapy. *ACS Appl Mater Interfaces*. 2019;11(23):20678–20688. doi:10.1021/acsami.9b04236
38. Jiang P, Hu Y, Li G. Biocompatible Au@Ag nanorod@ZIF-8 core-shell nanoparticles for surface-enhanced Raman scattering imaging and drug delivery. *Talanta*. 2019;200:212–217. doi:10.1016/j.talanta.2019.03.057
39. Zhong X, Zhang Y, Tan L, et al. An aluminum adjuvant-integrated nano-MOF as antigen delivery system to induce strong humoral and cellular immune responses. *J Controlled Release*. 2019;300:81–92. doi:10.1016/j.jconrel.2019.02.035
40. Luzuriaga MA, Welch RP, Dharmarwardana M, et al. Enhanced stability and controlled delivery of mof-encapsulated vaccines and their immunogenic response in vivo. *ACS Appl Mater Interfaces*. 2019;11(10):9740–9746. doi:10.1021/acsami.8b20504
41. Poddar A, Conesa JJ, Liang K, et al. Encapsulation, visualization and expression of genes with biomimetically mineralized zeolitic imidazolate framework-8 (ZIF-8). *Small*. 2019:e1902268. doi:10.1002/smll.201902268
42. Zhang H, Chen W, Gong K, Chen J. nanoscale zeolitic imidazolate framework-8 as efficient vehicles for enhanced delivery of CpG oligodeoxynucleotides. *ACS Appl Mater Interfaces*. 2017;9(37):31519–31525. doi:10.1021/acsami.7b09583
43. Liang Z, Yang Z, Yuan H, et al. A protein@metal-organic framework nanocomposite for pH-triggered anticancer drug delivery. *Dalton Trans*. 2018;47(30):10223–10228. doi:10.1039/c8dt01789a
44. Du Y, Gao J, Zhou L, et al. MOF-Based Nanotubes to Hollow Nanospheres through Protein-Induced Soft-Templating Pathways. *Adv Sci*. 2019;6(6):1801684. doi:10.1002/advs.201801684
45. Chen TT, Yi JT, Zhao YY, Chu X. Biomineralized metal-organic framework nanoparticles enable intracellular delivery and endo-lysosomal release of native active proteins. *J Am Chem Soc*. 2018;140(31):9912–9920. doi:10.1021/jacs.8b04457
46. Schafer M, Werner S. Oxidative stress in normal and impaired wound repair. *Pharmacol Res*. 2008;58(2):165–171. doi:10.1016/j.phrs.2008.06.004
47. Niethammer P, Grabher C, Look AT, Mitchison TJ. A tissue-scale gradient of hydrogen peroxide mediates rapid wound detection in zebrafish. *Nature*. 2009;459(7249):996–999. doi:10.1038/nature08119
48. Zhao BB, Guo HJ, Liu Y, et al. K313, a novel benzoxazole derivative, exhibits anti-inflammatory properties via inhibiting GSK3beta activity in LPS-induced RAW264.7 macrophages. *J Cell Biochem*. 2018;119(7):5382–5390. doi:10.1002/jcb.26685
49. Van de Velde F, Esposito D, Grace MH, Pirovani ME, Lila MA. Anti-inflammatory and wound healing properties of polyphenolic extracts from strawberry and blackberry fruits. *Food Res Int*. 2019;121:453–462. doi:10.1016/j.foodres.2018.11.059
50. Peng H, Geil Nickell CR, Chen KY, McClain JA, Nixon K. Increased expression of M1 and M2 phenotypic markers in isolated microglia after four-day binge alcohol exposure in male rats. *Alcohol*. 2017;62:29–40. doi:10.1016/j.alcohol.2017.02.175
51. Novak ML, Koh TJ. Macrophage phenotypes during tissue repair. *J Leukoc Biol*. 2013;93(6):875–881. doi:10.1189/jlb.1012512
52. Wynn TA, Vannella KM. Macrophages in tissue repair, regeneration, and fibrosis. *Immunity*. 2016;44(3):450–462. doi:10.1016/j.immuni.2016.02.015
53. Laplante P, Brillant-Marquis F, Brissette MJ, et al. MFG-E8 reprogramming of macrophages promotes wound healing by increased bFGF production and fibroblast functions. *J Invest Dermatol*. 2017;137(9):2005–2013. doi:10.1016/j.jid.2017.04.030
54. Zhang S, Liu Y, Zhang X, et al. Prostaglandin E2 hydrogel improves cutaneous wound healing via M2 macrophages polarization. *Theranostics*. 2018;8(19):5348–5361. doi:10.7150/thno.27385